An Investigation of the Thermal Response of Stationary Gas Tungsten Arc Welds

At 20% weld penetration, the weldment undersurface exerts an insulating effect on heat flowing through the thickness, with result that heat is retained in the metal and the increase in depth of penetration of the weld puddle accelerates with only slight increases in heat input

BY E. FRIEDMAN AND S. S. GLICKSTEIN

ABSTRACT. An analytical model developed to characterize the thermal cycle resulting from gas tungsten-arc welds is described and then used, in conjunction with a test program, to undertake an in-depth study of the effects of varying a number of welding parameters on the thermal response characteristics — in particular, the weld bead shape and depth of penetration.

The finite element method of analysis for transient heat conduction is employed to calculate temperatures in moderately thick NiCrFe Alloy 600 plates subject to a stationary GTAW heat source. Tests were run to provide data with which the computed thermal cycle can be correlated. The analytical model is then used to assess the effects on the weld bead shape and penetration of magnitude of heat input from the arc, distribution of the heat input over the surface of the weldment, and duration of the heat input. The finite element welding thermal analysis method is shown to be well suited for determining the interrelationship of these three factors on the thermal response. In particular, the potential for calculating the optimum combination of welding parameters for a given weld joint is demonstrated.

E. FRIEDMAN is a Fellow Engineer and S. S. GLICKSTEIN is a Fellow Scientist, Bettis Atomic Power Laboratory, Westinghouse Electric Corporation, West Mifflin, Pa.

Paper presented at the 57th Annual Meeting held in St. Louis, Missouri, during May 10-14, 1976.

Introduction

The development of effective welding techniques for a large number of metals and alloys has been the object of considerable effort. Concurrent with these developments, there have been attempts to identify and characterize the various problems that result from welding processes, and to establish criteria and guidelines for most effective joint design.

Information accumulated in these areas has been overwhelmingly experimental. Although attempts have been made to establish empirical approaches toward understanding the complex behavior of materials due to welding, comparatively little effort has been expended in developing and applying analytical models to explain and predict the welding transient thermal cycle. Most of the analytical methods that do exist deal with point, line or plane heat sources assumed to be concentrated in a body of infinite extent in one or more directions. The survey paper of Myers, *et al.* (Ref. 1) describes many of these methods.

Until recently, little effort was made to fully utilize the digital computer in order to eliminate many of the limitations inherent in the various concentrated source solutions. Numerical analysis enables such phenomena as temperature-dependent thermal properties, finite distribution of the heat source generated by the welding arc, latent heat effects, and irregular geometric shape of the workpiece and the weld bead, to be considered.

A paper by Hibbitt and Marcal (Ref. 2) represented an initial step in the development of numerical techniques to calculate both temperature transients and the resulting residual stresses. Both sets of calculations were carried out using the finite element method. Muraki, *et al.* (Ref. 3) employed the closed-form line source solution as input to a finite element analysis of metal movement in the plane of a thin welded plate. More recently, Paley and Hibbert (Ref. 4) made use of a three-dimensional finite difference program to describe the welding thermal cycle in both horizontal and vertical planes of welded plates. In all these papers, the primary objective has been to develop the analytical techniques and then to correlate the numerical results with experimental data.

In the present work, the finite element method of analysis is used to calculate temperatures in moderately thick plates resulting from a stationary gas-tungsten arc weld (GTAW) heat source. This represents the first phase of an analysis and test program for both stationary and moving arcs. In addition to correlating analytical and experimental temperature data, considerable effort

is made to utilize analytical tools to undertake an in-depth study of the effects on the thermal response of varying a host of parameters, as well as to assess the consequences of several assumptions required to set up the analytical model. Some preliminary work in this direction was reported by Glickstein, *et al.* (Ref. 5). Descriptions for calculating and measuring the weldment temperatures are presented first, followed by correlations of analytical and test data, and results of the parametric study.

Thermal Model

A complete description of the weld thermal model may be found in the paper by Friedman (Ref. 6). A summary of the salient features of the model and its application to the stationary arc weld presently under consideration is presented here.

The weldment analyzed is shown in Fig. 1, and is that of a 50.8 mm (2 in.) square plate, 6.35 mm (¼ in.) thick, of NiCrFe Alloy 600 whose material composition is described in Table 1.

The geometry of the analytical model is that of a section of the plate normal to its plane and passing through its center. Heat flow in regions removed from the plate edges is assumed axisymmetric about the center of the heat source, which is coincident with the center of the plate. Heat flow in the square plate is thus simulated by conduction in a 50.8 mm (2 in.) diameter circular plate. This assumption was validated by tracings taken from thermocouples located at the undersurface of the plate at the same distance from the weld centerline, but at different sections passing through the center.

Input parameters that are required for the analysis are the magnitude and distribution of the heat source from the arc and the duration of that source. The energy from the welding arc is, at any given time, assumed to be deposited on the surface of the weldment as a radially symmetric normal distribution function. The nature of energy deposition from the arc to the anode workpiece is discussed in a subsequent section. Letting Q (W) be the strength of the source, $\bar{r}$ (mm) the distance from the weld centerline, and $\bar{r}$ (mm) a heat distribution parameter defining the region in which 95% of the energy from the arc is deposited, the heat flux q_f (W/m²), acting on the weld surface, was given by Friedman (Ref. 6):

$$q_f(r, t) = (3Qt/\pi r^{-2}) \exp[-3(r/\bar{r})^2]. \quad (1a)$$

In the present work, calculations have been made for heat assumed to be applied both as a surface flux and as internal heat generated in a very thin layer adjacent to the anode (workpiece) surface. For the latter case, the heat generated is uniform through the thickness of the layer, and is given by:

$$q_i(r, t) = (3\,Qt/\pi r^{-2}h) \exp[-3(r/\bar{r})^{-2}] \quad (1b)$$

where h (mm) is the assumed thickness of the anode surface layer. In either case, Q represents the magnitude of the heat input, which is the product of arc current, voltage drop and arc efficiency, while $\bar{r}$ characterizes its distribution. The heat input rises linearly to its full value Q_o, after one-half second and is maintained uniformly until the power is cut off at some time t = t* (s). Thus,

$$Q = \begin{cases} 2tQ_o & 0 \le t \le 0.5 \\ Q_o & 0.5 \le t \le t^* \\ Q & t > t^*. \end{cases} \quad (2)$$

The finite element discretization in effect reduces the transient heat conduction equation, which is a partial differential equation, to a set of ordinary differential equations which contain time derivatives of temperatures at a discrete number of nodes — see, for example Wilson and Nickell (Ref. 7). A finite difference scheme is used to integrate these equations incrementally. The finite element method used for this analysis employs a biquadratic isoparametric element (Ref. 8), along each of whose sides the temperature may vary parabolically. The dimensions of the weld bead are defined by the liquidus isotherm, the location of which at any given time is found by interpolation of nodal point temperatures.

A direct iteration procedure for efficiently and accurately accounting for the latent heat absorbed during melting and liberated during solidification of the weld metal is employed in the analysis (Ref. 9). Temperature-dependent specific heat and thermal conductivity, and nonlinear boundary conditions are accounted for by specifying the material property and boundary coefficients for a given time step to be those evaluated at the beginning of the step. The coefficients are then updated for every time step.

On those surfaces not subject to heating by the arc, heat loss to the surroundings is effected by combined natural convection and radiation, as follows:

Table 1 — Chemical Analysis of Alloy 600, Wt-%

Ni	76.14	Co	0.08
Cr	15.27	S	0.005
Fe	5.76	P	0.018
Mn	0.34	Al	0.16
C	0.026	Ti	0.26
Cu	0.04	B	0.005
Si	0.20	Mg	0.01

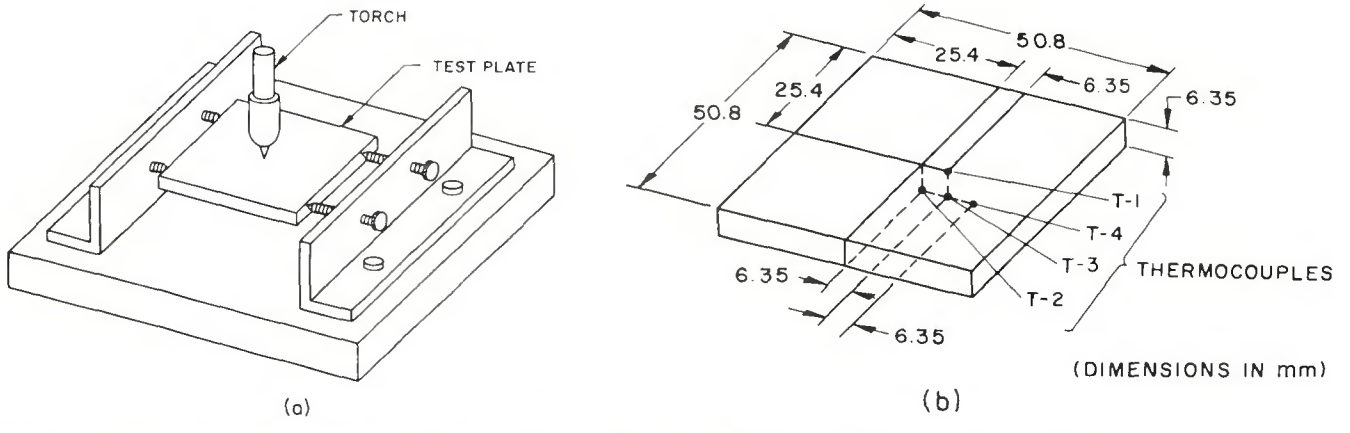

Fig. 1 — Experimental arrangement for: (a) left — holding the weld plate; (b) — thermocouple locations

$$-k\,\delta T/\delta n = 1.566\,(T - 480)^{1.25} + 5.68 \times 10^{-8}\,(T^4 - 295^4) \quad (3)$$

where k (W/m·K) is the thermal conductivity and $\delta T/\delta n$ (K/m) is the normal component of temperature gradient at the surface, and the two terms on the right hand side represent heat loss due to convection and radiation, respectively. This corresponds to natural convection losses into an atmosphere whose average temperature is 480 K and radiation losses to a body at 295 K. Properties of air are used to calculate the heat transfer coefficient for the former, while emissivity and shape factors are assumed to be unity for the latter.

The finite element mesh employed for the weldment cross-section is shown in Fig. 2. Only half the section is shown due to symmetry about the centerline. A relatively fine mesh is used in the vicinity of the centerline because of the very high temperature gradients expected in this region.

Experiment

A complete description of the experimental arrangement for measuring the plate temperatures is given in the paper by Glickstein, *et al.* (Ref. 5).

Very briefly, welds were made automatically using a gas tungsten arc electrode holder attached to a side beam welding fixture. The plates were held in place by four set screws as shown in Fig. 1a in order to eliminate the external heat sink that the usual clamping mechanism would have introduced. Chromel-alumel thermocouples were spot welded to various points on the top and bottom surface of the plate as is shown in Fig. 1b.

The temperature transient response was measured with a four channel chart recorder. The weld current and total voltage were recorded simultaneously and the arc voltage inferred from estimates of the line cable and electrode voltage drop (Ref. 5).

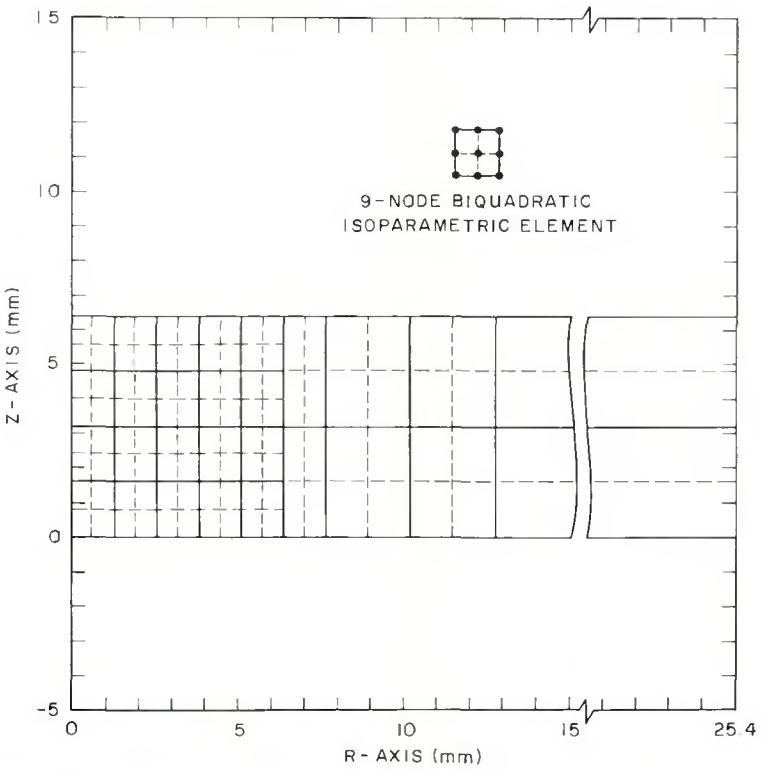

Fig. 2 — Finite element mesh

Comparison of Experiment and Calculation

Transient Temperature Response

The transient temperature response of the plate at thermocouple positions 1-4 (Fig. 1b) was measured and calculations performed for a given set of input energies. The results are shown in Fig. 3 for a weld current I = 91 A and an arc gap of 0.76 mm (0.03 in.). The recorded voltage V_r = 8.5 V. Assuming the line voltage drop V_l = 0.6 V and the drop in the electrode V_o = 0.25 V (Ref. 10), the arc voltage V_a = 7.7 V, and total arc power ($V_a \times I$) is 700 W. The duration of welding was 10 s.

The magnitude of the input energy was varied until agreement between experiment and calculation was obtained for the peak temperature at position T-2. Although such an

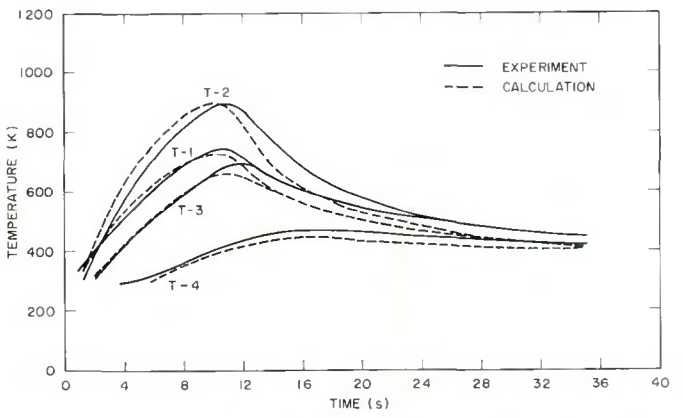

Fig. 3 — Comparison between calculated and experimental transient temperature response at four thermocouple positions. I = 91 A, V = 7.7 V, arc gap = 0.76 mm, hold time = 10 s, Q_o = 530 W, r^{-a} = 3.81 mm. Material properties used are indicated in Fig. 4

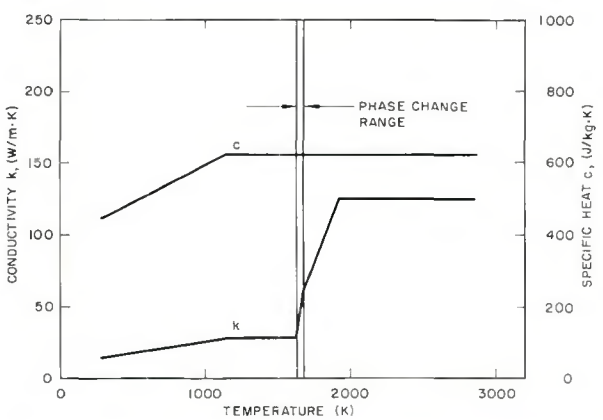

Fig. 4 — Material properties of Alloy 600 used for comparison of calculated and experimental thermal response. Density = 8415 kg/m³, latent heat = 309 kJ/kg

adjustment in the efficiency (defined as the thermal energy input divided by the total arc power) is arbitrary for this single point in time and position, the calculation reproduces the transient response during the entire heat-up and cool-down period reasonably well at all thermocouple locations on the plate when the efficiency is set equal to 0.76 (Fig. 3). For these calculations, Q_0 = 530 W and $\bar{r}$ = 3.81 mm — eqs (1) and (2). The material properties used are indicated in Fig. 4.

Because this example represents a "thick" plate condition, in that depth of penetration is a relatively small fraction of plate thickness, temperatures at locations T-2, T-3 and T-4, though not necessarily at T-1, are predominantly dependent on the total energy input and not on the details of the energy distribution. This is discussed further in the next section.

Although no measured puddle temperatures for Alloy 600 are known to the authors, it has been reported that the average puddle temperature may be estimated to be ~ 20% higher than the material's melting temperature of 1685 K (Ref. 11). While the temperature of the weld puddle was not measured in these experiments, its peak value was calculated to be ~ 2000 K at the center of the top surface of the plate. This is within the expected range.

Weld Metal Configuration

While the temperature transient response is reproduced analytically at points removed from the weld puddle, the computed melting isotherm which outlines the weld configuration needs improvement. In the case of a stationary arc weld, the cross-section of the weld puddle shown, for example, in Fig. 5 reveals a humped configuration. Such a configuration cannot be predicted analytically using any normal energy input distribution and standard heat conduction theory.

Further evidence which illustrates the difficulty in predicting weld metal configuration is displayed in the results of stationary arc welds taken for various weld times. Macrographs of these welds are shown in Fig. 6. Although the weld parameters are not precisely the same as those used to correlate the temperature transients discussed above, the calculated depth and width of the weld metal are nonetheless shown in Fig. 7 for heat input magnitudes of 530 W and 1060 W, along with the experimental data determined from Fig. 6.

The Q_0 = 530 W case produced satisfactory correlation of weld metal depth, while the Q_0 = 1060 W case resulted in the width being in good agreement with measured values. Nonetheless, the shape of the weld bead itself was not satisfactorily reproduced analytically. Further work into the heat transfer properties of the weld puddle accounting for weld puddle motion attributed to surface tension, arc jet forces, or Lorentz forces due to the current flow in the weldment, is clearly indicated.

Results of Parametric Study

The thermal response of a weldment depends essentially on three classes of variables:

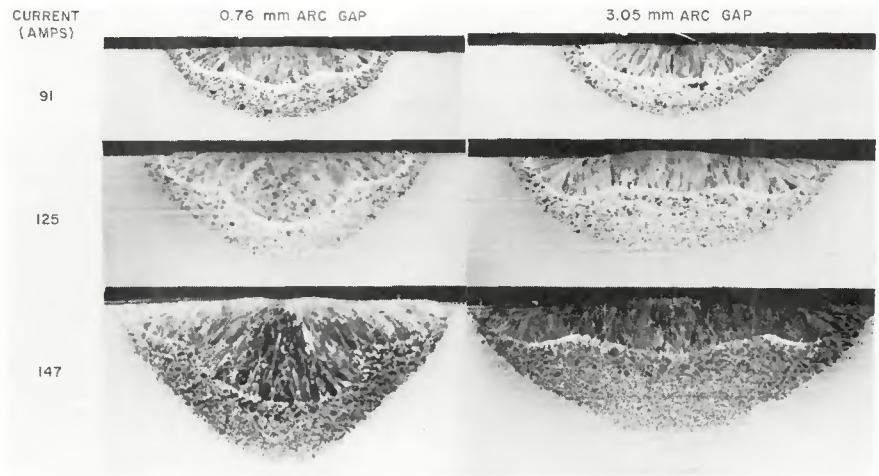

Fig. 5 — Cross-sections of stationary arc welds on 50.8 x 50.8 x 6.35 mm Alloy 600 plate. 10 second arc duration. X10 magnification (reduced 49% on reproduction)

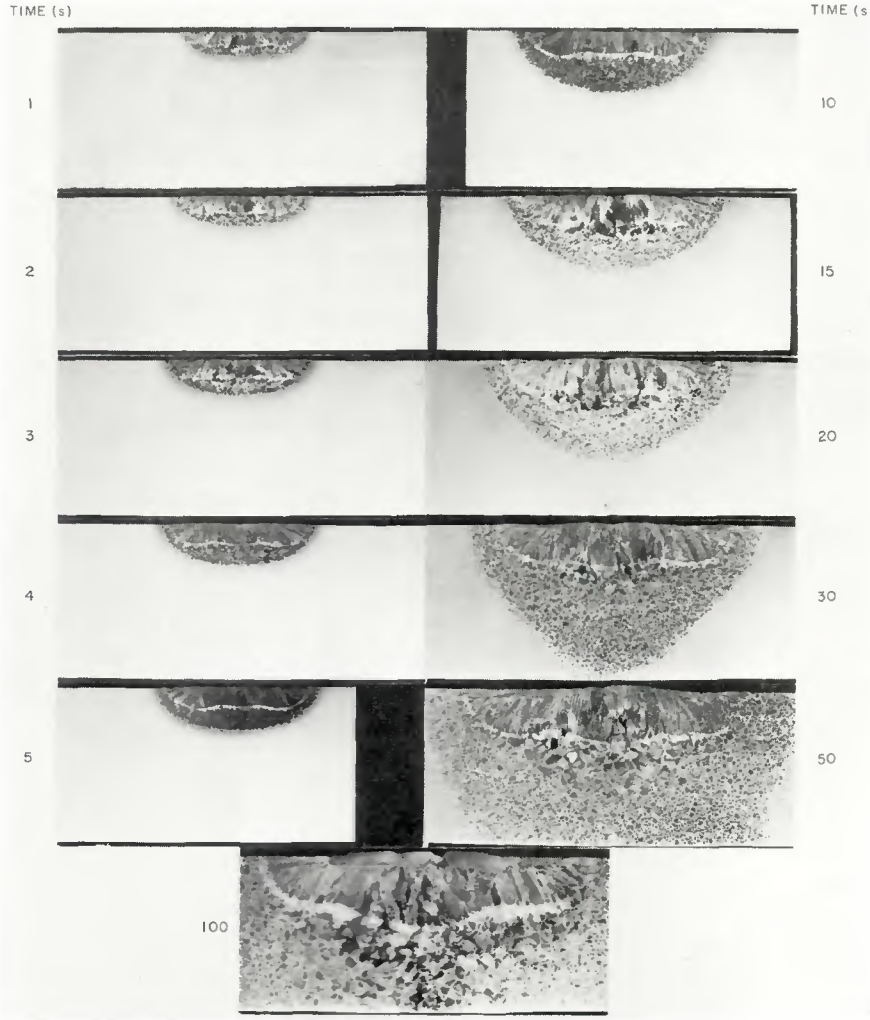

Fig. 6 — Weld configurations as a function of duration of heating

1. The heat input from the arc.
2. The heat transfer characteristics of the weldment.
3. The weldment geometry.

With respect to heat input from the arc to the workpiece, the magnitude of the heat input is obviously of prime importance. In addition to its effects on the temperature histories throughout the weldment and the weld bead penetration characteristics, the heat input magnitude relative to the thickness of the weldment determines whether a "thick" plate or a "thin" plate type of thermal response is obtained. The type of response, in turn, determines the nature of both the growth of the weld puddle as heat is added and the temperature distribution.

The distribution of heat input from the arc, although having only a relatively small effect on the thermal response in regions removed from the weld metal and heat-affected zones, has a significant influence on the geometry of the weld puddle. The precise nature of the heat input from the arc is also investigated by considering heat to be input as a flux on the surface of the weldment, and to be generated within a very thin layer adjacent to this surface, generally referred to as the anode surface.

Heat conduction characteristics for NiCrFe Alloy 600 are embodied in the thermal conductivity and specific heat, both of which vary with temperature, as well as the density and latent heat of melting. Temperature-dependent properties are known from room temperature to 1145 K (Ref. 12), and are shown by the solid lines of Fig. 8. Between 1145 K and the solidus temperature 1630 K, the conductivity and specific heat are assumed to take on their respective known values at 1145 K, as shown by the dashed lines of Fig. 8. The adequacy of this assumption is of course open to question, and only the experimental determination of the required high temperature data can serve to test its validity.

The characterization of heat transfer in the weld puddle itself is an even more formidable task. Until further work is undertaken and more is known about the mechanisms of heat flow in the puddle, only estimates of the molten metal thermal characteristics can be made by specification of appropriate values of conductivity and specific heat to be used in the analysis. These values, also indicated by dashed lines in Fig. 8, are intended merely to simulate puddle heat transfer, and in no way are meant to represent true conductivity and heat capacity of the molten metal.

On this basis, a study of the effects of both magnitude and directionality of puddle conductivity and magnitude of puddle heat capacity was undertaken. The latent heat of the alloy is taken to be that of nickel, which is 309 kJ/kg. Estimates of welding temperatures based on the use of solutions to point, line, or plane heat source problems always neglect the effect of latent heat. The consequences of doing this are also subject to investigation.

In addition to transferring heat away from the weld metal and heat-affected zones by conduction in the weldment, heat is also lost to the surroundings at surfaces not subject to direct heating by the arc — see eq (3). The consequences of significantly altering the appropriate surface heat transfer coefficient on the weldment thermal response have also been studied.

The geometry or weld thickness effects were not investigated directly, since the plate thickness of 6.35 mm (¼ in.) was maintained for all problems. However, the thickness effects were studied indirectly by considering both a relatively small heat input magnitude, which yields a partial penetration weld, and a heat input sufficiently large to eventually yield a full-penetration weld, in which the finite thickness of the weldment plays an important role in the evaluation of the thermal response.

The results of the parameter study involving all these variables are now presented. Keep in mind that the thermal response is characterized by the temperature histories at the four thermocouple locations shown in Fig. 1b, and by the width and depth of the weld puddle. The material properties used for all temperature calculations are shown in Fig. 8. Except for the study on weld puddle thermal properties, the effective molten metal properties employed are: c_1 = 1.377 kJ/kg•K, k_1 = 62.5 W/m•K, k_2 = 125 W/m•K.

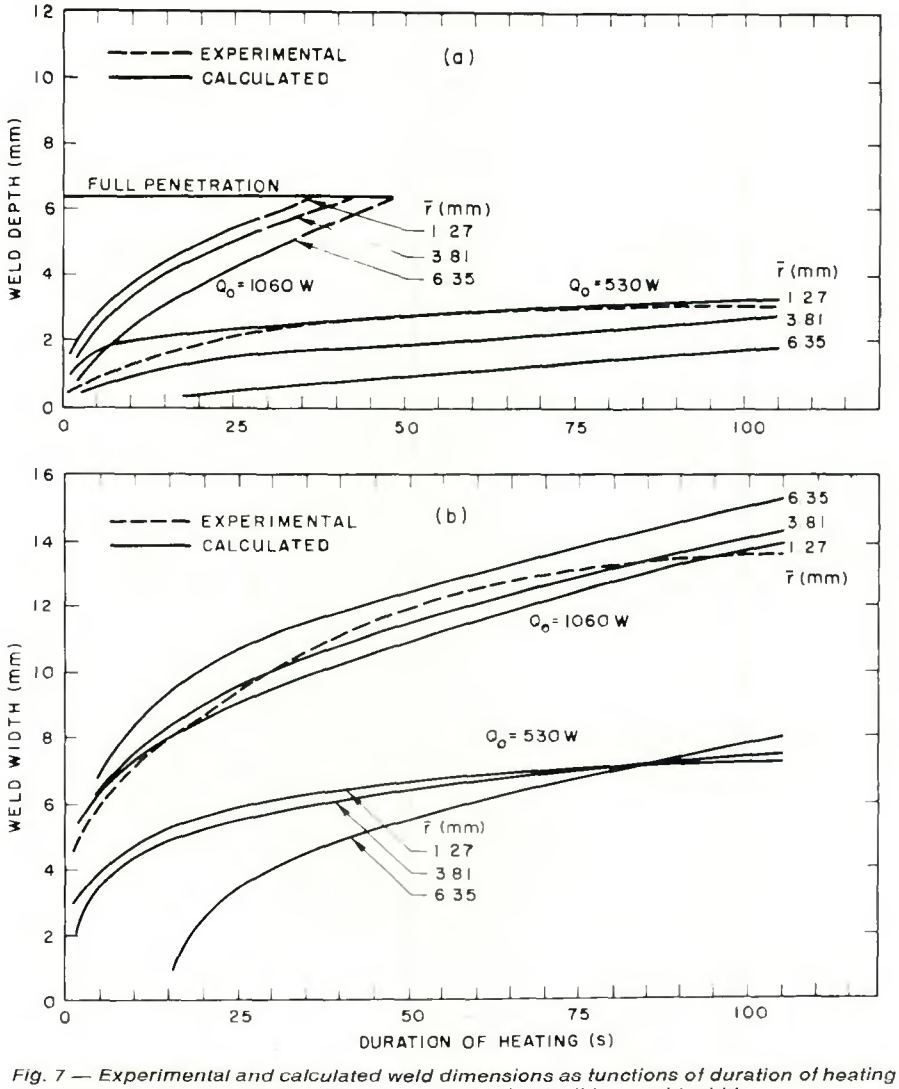

Fig. 7 — Experimental and calculated weld dimensions as functions of duration of heating for various heat input distributions. (a) — weld depth; (b) — weld width

Nature of the Heat Input from the Arc

In the GTA welding process, energy is transferred to the workpiece mainly by four mechanisms (Ref. 13):

1. Kinetic energy of the electrons comprising the arc current.
2. Heat of condensation of the electrons (work function) penetrating the solid work surface.
3. Radiation from the arc.
4. Thermal conduction from the arc plasma to the workpiece.

Because of the complicated nature in which the energy is actually dissipated in the workpiece, two different sets of initial boundary conditions specifying the heat source were considered. The first input heat from the arc as a flux, according to eq (1a), and the second input the heat internally in a thin layer adjacent to the anode surface according to eq (1b). Differences between the two sets of solutions were negligible. Thus, the choice of heat input mechanism is immaterial.

Magnitude of the Heat Input

The effects of varying the magnitude of the heat input Q_0 in eq (2) on the temperatures at the four thermocouple locations, as well as on the width, depth and volume of the weld puddle, are determined for a given duration of heating from the arc of 9.5 s. This was chosen because of its close proximity to the actual 10 s duration of arc heating of the test welds.

The curves of Fig. 9, which correspond to a heat input distribution parameter $\bar{r}$ = 3.81 mm (0.15 in.), show a linear variation of temperature with heat input magnitude at all thermocouple locations. Nonlinear effects are significant only in the vicinity of the puddle. At a heating duration of 9.5 s, the four thermocouple locations are too far removed from the puddle to effect any deviation from linearity.

Figures 10 and 11 show plots of puddle width, depth, and volume (the puddle shape is approximated by half a paraboloid for volume calculations) against heat input magnitude at 9.5 s of heat duration. Figure 10 is intended to illustrate the "thickness effect" with respect to weld puddle dimensions, by utilizing the closed-form temperature solutions existing for a point source of heat applied at the top surface of both a finite thickness and an infinite thickness plate. Details of the respective solutions are to be found in the Appendix.

For sufficiently low magnitudes of heat input, the point source on the surface of the finite thickness plate has the same effect as a source on an infinite thickness plate, and the half-width and depth of the puddle are therefore equal to each other. (Heat is radiated with spherical symmetry from the point source in an infinitely thick plate.) As heat input is increased, both the width and depth start to deviate from the infinite thickness plate solution. Thus, the "thickness effect" starts coming into play when the weld depth is about 20% of the plate thickness. At a puddle depth

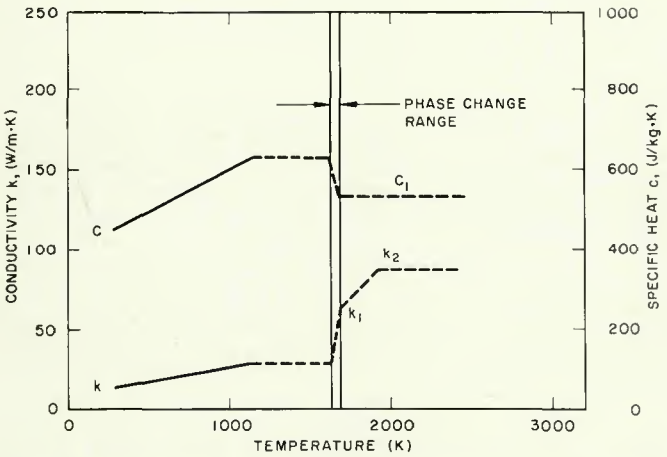

Fig. 8 — Material properties of Alloy 600 used for parametric study. Density = 8415 kg/m³, latent heat = 309 kJ/kg. k_1 and k_2 represent varied values of conductivity at temperatures 1685 K and 1920 K, respectively. C_1 is varied value of specific heat for $T \geq 1685$ K

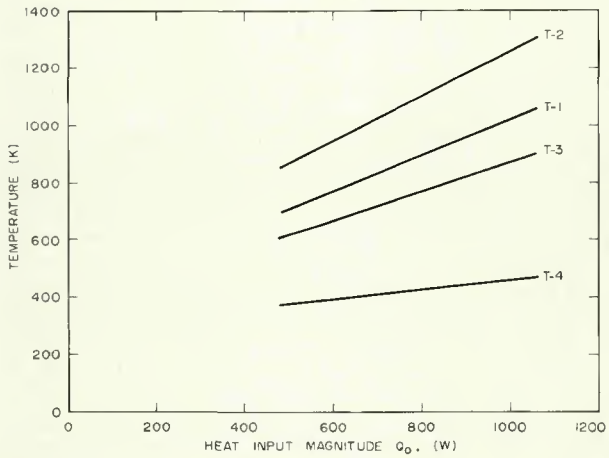

Fig. 9 — Variation of weldment temperatures at four thermocouple locations with heat input magnitude. Duration of heating = 9.5 s, heat input distribution parameter $\bar{r}$ = 3.81 mm

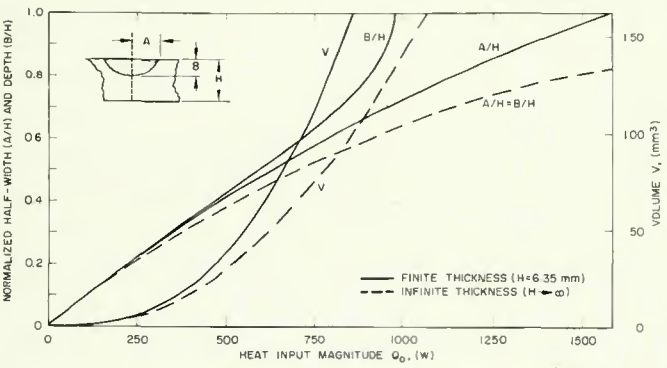

Fig. 10 — Weld puddle width, depth, and volume as functions of heat input magnitude for point source solutions. Duration of heating = 9.5 s

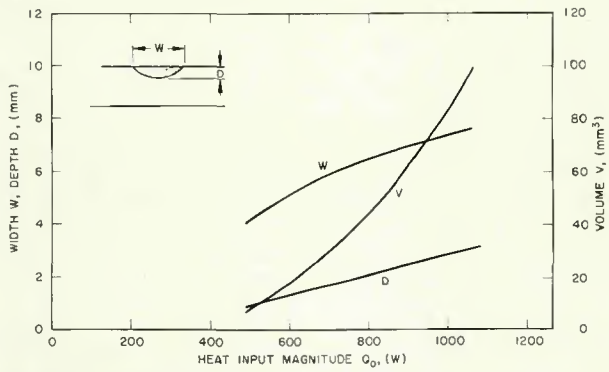

Fig. 11 — Effect of varying magnitude of heat input on weld puddle dimensions. Duration of heating = 9.5 s, heat input distribution parameter $\bar{r}$ = 3.81 mm

Fig. 12 — Heat input distribution and weld puddle shape for fixed magnitude Q_0 = 530 W and variable distribution parameter r. Duration of heating = 9.5 s. (a) $\bar{r}$ = 1.27 mm, (b) $\bar{r}$ = 2.54 mm, (c) $\bar{r}$ = 3.81 mm, (d) $\bar{r}$ = 5.08 mm, and (e) $\bar{r}$ = 6.35 mm

of about 60% of the plate thickness, the rate of increase of depth with heat input accelerates rapidly until a complete melt-through is attained.

Although the effect of plate thickness on puddle width is not as pronounced as on depth, the net effect on both puddle dimensions is manifested in the rate of increase of puddle volume with heat input. This rate deviates from that associated with the infinitely thick plate at very low penetrations and heat input levels. This serves to illustrate the undersurface of the weldment acting in effect as an insulation barrier and thus inhibiting the loss of heat by conduction away from the weld puddle. More heat is therefore retained in the neighborhood of the puddle and the puddle growth is accelerated. It is thus shown analytically that relatively little additional heat input is required to transform a partial-penetration weld to a full-penetration weld, when the bead depth of the former approaches the thickness of the plate.

The nature of puddle growth in a real weld differs from that obtained using the point source solution, primarily because of the finite area over which the heat input is applied. For the curves plotted in Figure 11, this area corresponds to a heat input distribution parameter $\bar{r}$ = 3.81 mm (0.15 in.). The distributed source has the effect of inhibiting penetration and making the puddle more shallow.

Other phenomena not accounted for in the point source solution that affect the magnitude of weld depth, width, and volume include heat losses by convection and radiation at surfaces not subject to heating from the arc and latent heat of melting. The effects of heat input distribution, surface losses and latent heat are discussed elsewhere in this paper.

Distribution of the Heat Input

The effects of varying the distribution of the heat input, characterized by the parameter $\bar{r}$ in eq (1), on the weldment thermal response depend on the duration of heating and the magnitude of the heat input as well. To illustrate the manner in which the distribution of heat influences the size and shape of the weld bead, consider the case in which the heat input magnitude Q_0 = 530 W. At 9.5 s the shape of the weld puddle cross-section is shown in Fig. 12 for $\bar{r}$ = 1.27, 2.54, 3.81, 5.08 and 6.35 mm (0.1, 0.15, 0.2 and ¼ in.). Also shown is the distribution of heat input (piecewise constant due to the necessity of heat generated uniformly within each finite element), considered to be applied within a 0.3175 mm thick layer adjacent to the anode surface. The effect of distribution on penetration is evident.

Since Fig. 12 corresponds to a specified set of values for heat input magnitude and duration of heating, the effects of heat input distribution on weld bead width and depth for a number of specified heating durations were determined for two sets of heat input magnitudes. The results of this study are plotted in Figs. 13 and 14 for Q_0 = 530 W and Q = 1060 W, respectively. It is seen that both heat input magnitude and duration of heating strongly influence the weld bead variation with $\bar{r}$. The amount of heat H, generated in the anode surface layer is expressed simply as:

$$H = \int_0^{t^*} Q \, dt \qquad (4)$$

where Q is given by eq (2), regardless of the distribution parameter $\bar{r}$. Thus for a relatively small heat input magnitude Q_0, and heating duration t*, the total heat supplied must be concentrated in a very small region in order to produce any melting at all.

From Figs. 13 and 14, it is seen that for relatively short time durations, the depth (or penetration) of the weld bead as well as the bead width decrease as the heat input becomes more diffuse. For sufficiently large values of $\bar{r}$, no melting can be initiated at all. As the duration of heating and, therefore, the total heat input, is increased, melting can be initiated at the anode surface for increasing values of $\bar{r}$. Although in all cases the weld bead depth decreases with increasing $\bar{r}$, the bead width can, for sufficiently high durations of heating, increase with increasing $\bar{r}$, and continue increasing until some level of heat input distribution is reached that can no longer sustain melting on the anode surface, whereupon the bead width decreases rapidly with any further increases in $\bar{r}$.

This phenomenon comes about due to the availability of sufficient energy to initiate melting on the anode surface even though that energy is distributed over an increasingly larger area of that surface. Eventually, however, the anode surface area over which heat is generated becomes so large that, regardless of the magnitude of the heat input, there is not enough heat generated per unit surface area to get that area hot enough to initiate melting. The value of $\bar{r}$ at which the weld bead width is a maximum naturally increases with both the duration of heating and the magnitude of the heat input. Thus, when assessing the effects of heat input magnitude, heat input distribution and duration of heating on the shape and size of the weld bead, the complex interaction of the three parameters must be considered.

Characteristics of Full-Penetration Weld

For the high heat input case of Q_0 = 1060 W, the weld puddle completely penetrates the plate after a given duration of heating, the value of which depends on the distribution parameter $\bar{r}$. The effect of $\bar{r}$ on the dimensions of a full-penetration weld is illustrated in Fig. 15, in which a number of temperature contours are plotted for t* = 42 s, and for the values of $\bar{r}$ of 1.27 and 6.35 mm.

The difference in puddle or weld bead shape is evident. Observe also

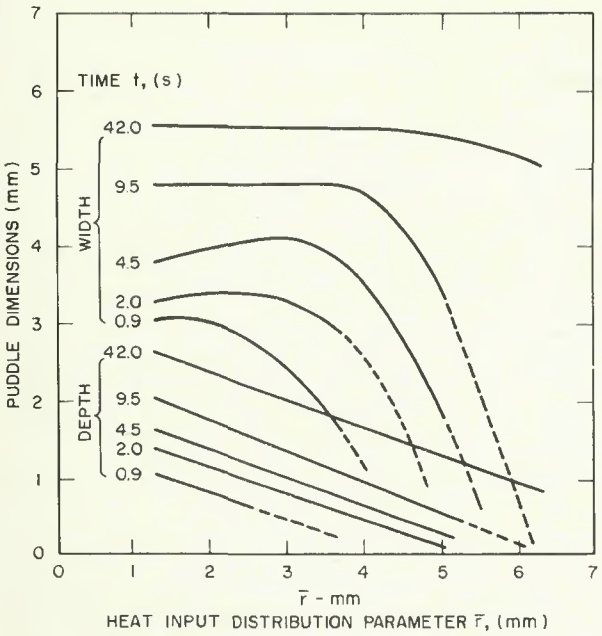

Fig. 13 — Weld puddle dimensions for different durations of heating t, and heat input distribution parameters r̄. Q_0 = 530 W

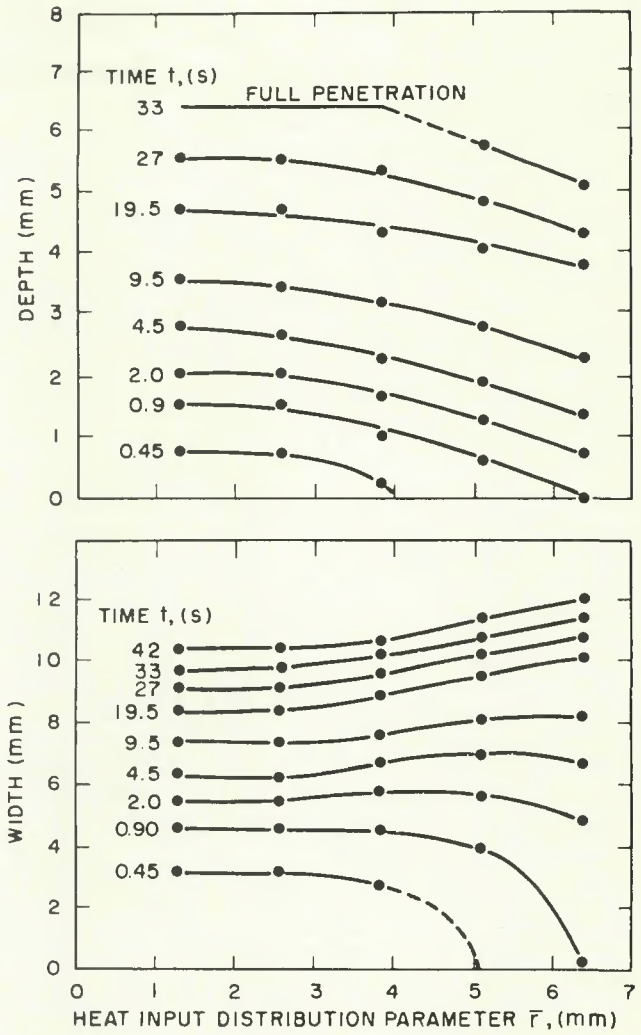

Fig. 14 (right) — Weld puddle dimensions for different durations of heating t, and heat input distribution parameters r̄. Q_0 = 1060 W

that for all regions of the weldment, with the exception of that near the weld centerline on the undersurface, higher temperatures result for the wide distribution case, i.e., r̄ = 6.35 mm (0.25 in.). This shows that a more concentrated heat source results in more heat being lost to the surroundings at the undersurface of the weldment near the molten region.

The variation of the bottom surface width with the distribution parameter for various heating durations is shown in Fig. 16. The same general type of behavior observed for the top width variation applies here as well. The growth of the full-penetration weld at the top and bottom surface for extreme values of r̄ is shown in Fig. 17. For relatively short times, the more concentrated heat source produces a wider weld puddle. As the duration of heating is increased, sufficient heat is being supplied to enable the more widely distributed heat input to generate a wider puddle.

The effect of heat input distribution on temperature histories at locations somewhat removed from the weld puddle is less dramatic. Figure 18 shows plots of peak temperature against distribution parameter at the four thermocouple locations for the case in which heat is supplied from the arc for 10 s. The distribution effect is most pronounced at the two thermocouple locations nearest the weld puddle (T-1 and T-2), while it is less evident at T-3 and negligible at T-4. At T-1 on the top surface, an increasing r̄ tends to raise the peak temperature. This has been observed experimentally and discussed previously (Ref. 5). At the location of T-2 at the bottom surface, the opposite effect is observed.

Effect of Surface Heat Losses

Conditions at weldment surfaces not being heated directly by the arc influence the amount of heat lost to the surroundings at these surfaces and, to some extent, the temperature transients and the weld bead dimensions (Ref. 14). To make a qualitative assessment of this effect, the natural convection heat transfer coefficient (included in the first term of the right hand side of eq (3) of 1.566 W/m²• $K^{1.25}$ was arbitrarily increased by a factor of 30 to 47 W/m² • $K^{1.25}$. No changes were made with regard to surfaces losses due to radiation.

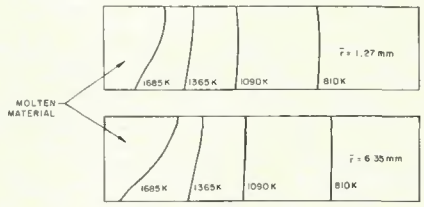

Fig. 15 — Effect of heat input distribution parameter r̄ on weld puddle shape and temperature contours. Q_0 = 1060 W, duration of heating = 42 s

As expected, the higher heat transfer coefficient results in lower temperatures throughout the weldment, as shown in Fig. 19. The effect on the bottom surface is greater as the distance from the weld centerline is increased, as seen from the temperature plots at thermocouple locations 2, 3, and 4 (Fig. 1). This arises due to surface heat losses that are maximum at the weld centerline.

These losses, although resulting in

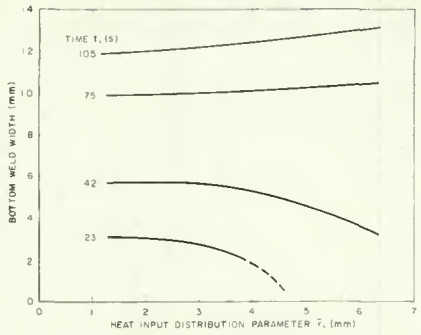

Fig. 16 — Bottom width of full-penetration weld as a function of heat input distribution parameter $\bar{r}$, and duration of heating t. Q_0 = 1060 W

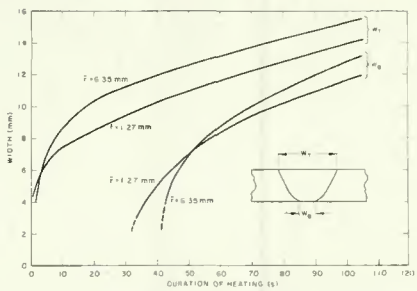

Fig. 17 — Weld puddle widths as functions of duration of heating and heat input distribution parameter $\bar{r}$. Q_0 = 1060 W

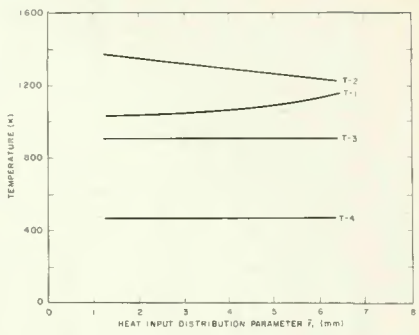

Fig. 18 — Calculated peak temperatures at four thermocouple locations as functions of heat input distribution parameter $\bar{r}$. Q_0 = 1060 W

a decreased temperature at the weld centerline, also cause a smaller fraction of heat to be conducted away from the center region of the weldment to the cooler regions. A combination of this lesser amount of heat being conducted to the cooler regions and more heat being lost to the surroundings due to the increased surface heat transfer coefficient yields greater decreases in temperature as the distance from the weld centerline is increased.

Figure 19 shows that the surface heat loss effect becomes significant for durations of heating that are sufficient to raise the temperatures at the undersurface of the weldment at the weld centerline to a rather high level. At this level, the "thin" plate type of thermal response comes into play, and the effects on weld puddle dimensions and penetration become significant. This is shown in Fig. 20, in which puddle width and depth are plotted against duration of heating, and in Fig. 21, which depicts temperature contours for the two cases at a heating duration of 42 s.

Although the imposed increase in heat transfer coefficient by a factor of 30 may be somewhat drastic, it does serve to illustrate the importance of surface conditions on weldment temperatures and penetration characteristics. Such conditions may actually be present if there exists any gas flow at the undersurface of the weldment. A backing material or thin insulating film may act in the opposite sense.

Thermal Properties in the Weld Puddle

Heat transfer in the weld puddle is simulated by specification of effective thermal conductivity k (magnitude and directionality), and the product of density and specific heat pc. The specific parameters used to characterize the effective puddle properties are described in Fig. 8.

All parameter variations were carried out using a heat input magnitude of either 490 or 530 W, and a heat input distribution parameter value of 3.81 mm (0.15 in.). Under these conditions, there were no significant changes in temperature at any of the four thermocouple locations for any of the effective puddle property variations. This discussion is therefore limited to the effects of these variations on weld dimensions and on maximum puddle temperature, calculated on the weld centerline at the top surface.

With the effective isotropic puddle conductivities of k_1 = 62.5 W/m•K and k_2 = 125 W/m•K (see Fig. 8), the effective specific heat c, in the puddle was varied between 0.276 and 1.377 kJ/kg•K, a range within which the specific heat of the solid material is included. No perceptible variations of the weld bead dimensions were calculated for Q_0 = 490 W and a duration of arc heating of 10 s. The maximum puddle temperature does, however, decrease from 2100 K to 1895 K as c is increased. These peak temperatures exceed the melting temperature of Alloy 600 by 30% and 15%, respectively. This is within reasonable agreement of the average puddle temperature, which is expected to be ~ 20% higher than the melting temperature (Ref. 11).

The effects of the magnitude of the effective puddle conductivity on the weldment thermal response were calculated using a heat input magnitude of 490 W and a heating duration of 10 s. The specific heat c, in the puddle was fixed at 0.624 kJ/kg•K. The initial set of calculations was made assuming puddle conductivity to be isotropic and equal to 29 W/m•K, which is the conductivity of the solid metal. This produced a peak puddle temperature of 2245 K, which exceeds the melting point by 40%.

In an attempt to reduce the puddle temperatures to more reasonable levels, the effective conductivity was increased by varying amounts. Since an infinite puddle conductivity would theoretically produce a uniform distribution of temperature whose magnitude is that of the melting point, an arbitrarily high value of puddle conductivity of 1.2 x 10^9 W/m•K was used. This produced transient temperature oscillations that rendered the solution useless. These oscillations arise because of the extremely rapid increase in conductivity from the solidus temperature 1630 K, to the liquidus 1685 K, which results in a virtual discontinuity of temperature gradient at the liquid/solid interface.

Since, for the presently employed finite element method, the temperature is the dependent variable, continuity of temperature gradient within, but not on the boundary of, each finite element is guaranteed (Ref. 6). This results in the melting isotherm progressing through the weldment discontinuously and causing temperatures in and around the puddle to oscillate with time.

Attempts were made to reduce the magnitude of these oscillations and yet maintain the peak puddle temperature at a reasonable level by lowering the puddle conductivity from 1.2 x 10^9 W/m•K to 1250 and then to 625 W/m•K. The results were also unsatisfactory. The conductivity was altered again, so that k_1 = 125 W/m•K and k_2 = 1250 W/m•K (see Fig. 8). This again produced unsatisfactory oscillations. Finally k_1 and k_2 were reduced to 62.5 and 125 W/m•K, respectively. At these values, the maximum oscillation was 70 K, and a peak puddle temperature of 2055 K, which exceeds the melting temperature by 27%, was obtained. Both are acceptable and these effective conductivity parameters were used for subsequent calculations.

The conductivity parameters referred to are isotropic — that is, they

are the same in all directions. On this basis, heat input parameters of Q_0 = 530 W applied for 10 s and $\overline{r}$ = 3.81 mm produced a weld bead width and a depth of 4.3 and 1.0 mm, respectively. This compares with corresponding bead dimensions of the test weld of 5.9 and 1.2 mm.

In an effort to reduce the width/depth ratio of the computed weld bead while at the same time maintaining the heat input so that the temperatures calculated at the thermocouple locations would not change, the conductivity was made anisotropic. This was done such that the radial components of the conductivity parameters k_1 and k_2 were kept at 62.5 and 125 W/m•K, respectively, while the corresponding parameters in the thickness direction were reduced to 12.5 W/m•K. It was hoped that the introduction of an effective anisotropic puddle conductivity would result in improved simulation of heat flow in the puddle.

Anisotropic puddle conductivity resulted in the weld bead width being increased from 4.3 to 5.3 mm and the depth decreased from 1.0 to 0.8 mm. The width/depth ratio was therefore increased from 4.3 to 6.6. This compares to 4.9 for the test weld. Though the desired effect of increasing the width/depth ratio of the weld bead was obtained, the increased bead width resulted in a decreased weld depth. Therefore, simulation of heat transfer in the puddle by an effective anisotropic conductivity, though serving to increase the weld/depth ratio, does little to make the calculated bead dimensions approach the measured values in the test weld.

It seems apparent that simulation of heat flow in the weld puddle for a stationary arc weld cannot properly be carried out using an exclusively conducting model. It is worth noting, however, that this conclusion applies only to stationary arc welds, where the unusual humped configuration is obtained. Further analysis and testing is required prior to coming to any conclusions regarding moving welds, where the weld bead configuration appears to have a more normal appearance (Ref. 5).

Latent Heat Effect

The importance of including the latent heat of melting in a welding thermal analysis was tested by considering conditions which result in a full-penetration weld: Q_0 = 1060 W, $\overline{r}$ = 3.81 mm (0.15 in.). Temperatures and weld bead dimensions were calculated for the cases in which the latent heat is 309 kJ/kg and the latent heat is such that there is no increase in the heat capacity of the material in the phase change range bounded by the solidus and liquidus temperatures. The latter has the effect of neglecting the consequences of latent heat — see, for example, the literature (Ref. 9) for a mathematical definition of latent heat.

The latent heat effects are illustrated in Fig. 22, in which weld puddle width and depth are plotted against time for both cases. The effect on puddle dimensions is most pronounced when conditions for a full-penetration weld are approached or met. This is further illustrated by Fig. 23, which shows temperature contours for the two cases after a duration of heating of 27 s. The importance of including latent heat effects in a welding thermal analysis is thus evident for "thin" weldment conditions, and less important for "thick" plate conditions.

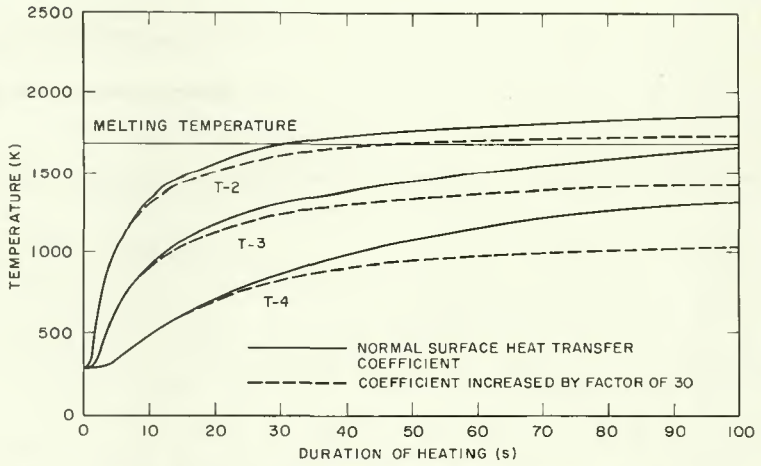

Fig. 19 — Effect of surface heat losses on temperatures at thermocouple locations 2, 3 and 4 on undersurface

Discussion

An in-depth study of the welding thermal cycle for gas tungsten-arc welds has been undertaken in two phases — the first dealing with stationary sources of heat and the second with moving arcs. For the first phase of this effort, comparisons were made between the results of a transient temperature analysis and corresponding experimental data for a 91 A, 7.7 V stationary arc applied for 10 s to a 6.35 mm (0.25 in.) thick Alloy 600 plate.

Assuming an arc efficiency of 0.76, good correlation between calculated temperatures and thermocouple readings was obtained at a number of locations outside of the weld metal and heat-affected zones. The test welds produced a humped weld metal configuration that could not be produced analytically. Since this odd configuration has been observed only for stationary welds, this may not be of any concern in the phase two study of moving welds. Although the width/depth ratio of the weld metal cross-section of the test weld is not in very good agreement with the calculated ratio, reasonable correlation is obtained for the depth of penetration.

The comparison of analytical results with test data for a relatively simple weldment leads one to conclude that the finite element numerical approach taken here to calculate the welding thermal response can be used with a high degree of confidence to investigate the relative effects of a number of welding parameters and conditions on the thermal cycle. In particular, the effects on depth of penetration, shape and size of the weld metal region, temperature transients, and cooling rates are of concern. The stationary heat source phase of this study enabled the consequences of varying the weld parameters (with the exception, of course, of the weld speed), the weldment thickness, and other weld characteristics to be assessed.

The question of the precise means by which heat is input to the weldment from the arc has been addressed by running sets of problems with heat input characterized both as a surface flux on the anode surface, and as heat generated within a thin layer of material adjacent to the anode surface. Since it was found that the choice of the heat input mechanism is immaterial, one need not be concerned with this question for analytical purposes.

One of the more fundamental results of this study is the ability to demonstrate analytically and quantitatively the profound effects of the thickness of a weldment, relative to the heat input, on the weld bead configuration and temperature transients. The influence of thickness

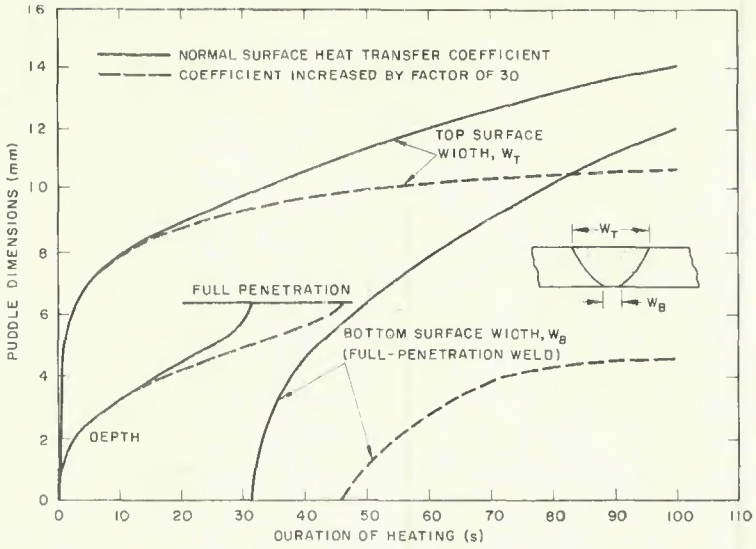

Fig. 20 (left) — Effect of surface heat losses on puddle dimensions

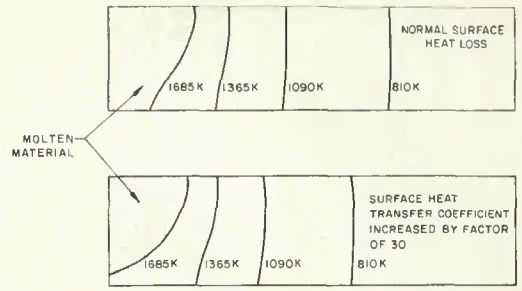

Fig. 21 — Effect of surface heat losses on weld puddle shape and temperature contours. Q_0 = 1060 W, duration of heating = 42 s

on penetration characteristics is especially illuminating. The effect of weldment thickness has been shown to become important with respect to characterizing weld penetration when the depth of penetration is only 20% of the thickness. At this point, the undersurface of the weldment begins to exert an insulating effect on the heat flowing through the thickness. Thus heat is retained in the metal and the increase in depth of penetration of the weld puddle is accelerated as the magnitude of heat input is increased. At about 60% penetration, it is shown that the puddle depth increases rapidly until full penetration is achieved, though the heat input is increased only slightly.

In test welds and weld mockups, it has often been observed that the difference between a partial-penetration and a full-penetration weld results from an increase in current of just several amperes. The weld thermal analysis has been shown to completely characterize this phenomenon. These results also lead to the conclusion that, when attempting to identify certain characteristics of a welded joint by performing bead-on-plate welds, the thickness of the test weld must be in line with the actual thickness of the weldment for which the test results are to be applied. In other words, if the weldment to be made is 2 mm (0.08 in.) thick, test welds to determine characteristics of the welding process should not be performed, say, on 6 mm (0.24 in.) thick plates. The fundamental differences that exist between "thick" and "thin" weldments with respect to the welding thermal response have thus been characterized.

The energy available during welding is often characterized by the product of the arc current and voltage. (The voltage must be carefully defined in order to make proper comparisons between various sets of experimental data.) Multiplication of this number by some efficiency factor yields the magnitude of the thermal energy transmitted to the workpiece. Even neglecting the effects of weld speed for this first phase study, it has been demonstrated that the magnitude of the heat input alone is inadequate to determine depth of penetration and weld bead shape.

In order to maximize penetration and optimize weld bead shape, the distribution of the heat input, coupled with the heat input magnitude and the weldment thickness, must be considered. Due perhaps to lack of knowledge regarding the size of the anode surface area upon which significant amounts of heat are deposited via the arc, the effects of distribution of the input energy have received only cursory attention. With the analytical tools now available, criteria can now be developed for determining what combinations of heat input magnitude and distribution are required to give an optimum weld configuration for a weldment of given thickness.

Data have been generated for weld depth and width to illustrate the changes in weld dimensions that take place in a stationary weld of 6.35 mm (0.25 in.) thickness as the magnitude, duration, and distribution of the heat input are varied. The means for performing analytical studies of this sort for other weld configurations and for moving welds when the additional parameter of weld speed is included, is thus established. It has also been demonstrated that, under fixed conditions of heat input magnitude and duration, the difference between a partial penetration and a full penetration weld can depend only on the area upon which the heat is distributed.

The means for specifying the welding heat input parameters required to produce an optimum weld configuration have thus been established analytically. The question remains as to how these parameters may be effectively controlled by varying the welding parameters (current, voltage, arc gap, electrode shape, etc). This presents an extremely difficult problem. In the GTAW process the electric arc serves as the conductor for transmitting energy to the weld plate. Because of the complex manner in which the arc establishes its equilibrium state, it is difficult to predict precisely the influence various welding conditions will have upon the arc discharge. For example, vapors are emitted into the arc from the weld puddle at some unknown rate determined by the base material, its impurities, and heat input to the weld surface. Depending upon the nature of the vapors, the characteristics of the arc may change resulting in changes in the arc temperature, configuration, and ultimately upon the heat input to the weldment, itself (Ref. 15).

Other parameters such as electrode configuration, shielding gas, arc gap, etc. may also exert a profound influence upon the arc. In order to characterize the heat input distribution and thus be able to optimize and control weld bead configuration, continuing studies of the welding arc are essential.

Calculation of the welding thermal cycle for a given set of welding conditions depends to some extent on the

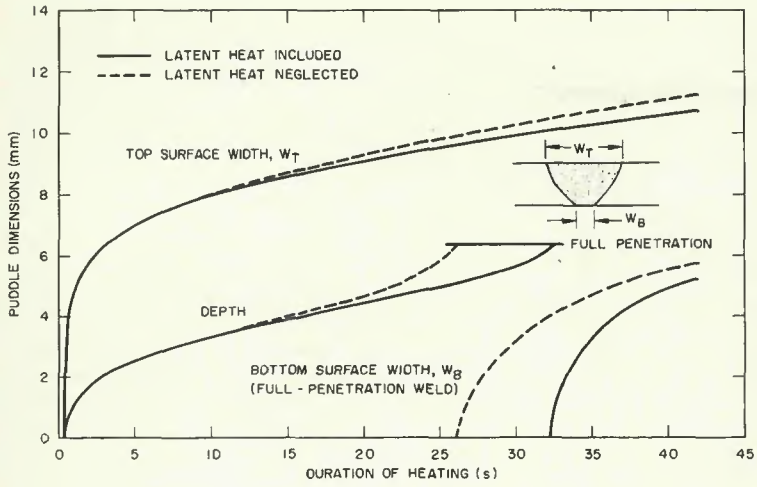

Fig. 22 (left) — Effect of latent heat on puddle dimensions

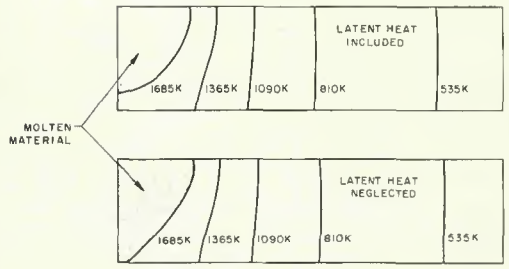

Fig. 23 — Effect of latent heat on weld puddle shape and temperature contours. Q_0 = 1060 W, duration of heating = 27 s

heat loss conditions at weldment surfaces not subject to direct heating by the arc. These heat loss conditions, which are specified analytically as combined losses due to natural convection and radiation, are difficult to evaluate and are subject to some degree of uncertainty.

The sensitivity of the thermal response to variations in the surface conditions was assessed. For welding conditions in which the "thin" plate type of thermal response comes into play, the sensitivity becomes significant. Although further effort is required to get a better handle on surface heat loss conditions to be expected in actual welds, it has been demonstrated analytically that a thirty-fold increase in the natural convection surface heat transfer coefficient very dramatically decreases weld penetration. For welding procedures that make use of backing materials, the welding thermal analysis procedure is very well suited for evaluation of various materials and their thicknesses, since they can be characterized by effective surface heat transfer coefficients.

Due to motion of molten material, heat transfer in the weld puddle cannot be completely described by conduction alone. Until further work is undertaken to characterize heat flow in the puddle, effective values of heat capacity and conductivity are specified to simulate the actual heat transfer mechanisms. The criteria for adequate simulation of these mechanisms are the calculation of reasonable levels of puddle temperature, stability of the numerical temperature solution, and satisfactory prediction of depth of penetration and width of the weld metal.

Peak puddle temperatures that exceed the melting point of Alloy 600 by about 20% have been obtained with no detrimental effect on the numerical stability of the temperature solution. Effective molten metal specific heat on the order of the specific heat of the solid material, together with an effective puddle conductivity that exceeds somewhat the solid material conductivity, produces these results. Lower conductivity results in puddle temperatures that are too high, while higher conductivity yields an unstable solution.

In an attempt to adjust the weld metal width/depth ratio to yield the more shallow weld metal region that was observed experimentally, anisotropic puddle conductivity was introduced, such that there would be a greater propensity for heat to be transferred parallel to the plane of the weldment than in the thickness direction. Anisotropic conductivity did indeed produce an increased width/depth ratio; however, the greater weld metal width was developed in conjunction with a lower depth. Both calculated weld bead dimensions remained, however, below the corresponding measured values, thus making it clear that, at least for stationary welds, heat flow in the puddle cannot be completely simulated using an analytical model that accounts only for heat transfer by conduction.

Analytical treatments of welding heat conduction that utilize point, line or plane sources of heat in order to develop closed-form temperature solutions neglect effects of latent heat. The consequences of doing this in a welding thermal analysis were investigated. The results of this study show that, when analyzing a weld in which conditions for full penetration are approached or met, the inclusion of latent heat in the calculations significantly affects the weld configuration.

Conclusions

An analytical and experimental investigation of the welding thermal cycle for stationary gas tungsten-arc welds has led to the following results:

1. The welding thermal analysis model, in conjunction with the finite element method for transient heat conduction analysis, produces a thermal cycle that is in very good agreement with thermocouple data at locations outside the weld metal and heat-affected zones.

2. Although calculated depth of penetration of the weld is in line with depths measured from metallographic sections, the humped, shallow weld metal configuration observed for stationary test welds cannot be reproduced analytically. Introduction of anisotropy of the effective puddle conductivity, although producing a more shallow weld bead, results in bead dimensions that are smaller than the measured values.

3. Heat transfer exclusively by conduction is inadequate to completely characterize thermal conditions in the weld puddle and thus to accurately predict both depth of penetration and width of the weld metal cross-section. Additional work on puddle heat transfer is required to shed more light on this area.

4. The nature of the weldment thermal response and the resulting weld bead penetration and shape characteristics are very much dependent on the thickness of the weldment relative to the heat input from the arc. The differentiation between "thin" and "thick" weldment types of thermal response is crucial for proper interpretation of any experimental or analytical welding analysis. When attempting to identify certain characteristics of a welded joint by perform-

ing bead-on-plate welds, the thickness of the test weld must be compatible with the actual thickness of the weldment for which the test results are to be applied.

5. The analytical model vividly demonstrates that, for a weld whose depth of penetration is as low as 60% of the thickness, a small increase in current can produce a full-penetration weld.

6. In addition to the magnitude of the heat input from the welding arc, the area over which that heat is distributed on the anode surface is an additional parameter that strongly influences penetration and weld bead shape characteristics.

7. The finite element welding thermal analysis method is very well suited for determining the interrelationship of heat input magnitude, heat input distribution, duration of the heat input, and weldment geometry on the thermal response. In particular, it can be used for calculating that combination of thermal and geometric parameters that will produce an optimum weld configuration for a given joint.

8. Although the means have been established to specify magnitude and distribution of the heat input from the arc so that an optimum weld metal configuration and weldment thermal response will be obtained, the problem remains as to how these parameters may be controlled by varying specific welding parameters such as current, voltage, electrode shape, arc gap, shielding gas, and insert additives. Continued effort on the nature of the welding arc is essential for developing criteria for these parameters.

Acknowledgment

The authors wish to acknowledge the contributions of Ms. Y. B. Turchan, who ran the numerous computer jobs and helped reduce the data.

References

1. Myers, P. S., Uyehara, O. A., and Borman, G. L., "Fundamentals of Heat Flow in Welding," Welding Research Council Bulletin No. 123, July 1967.

2. Hibbitt, H. D., and Marcal, P. V., "A Numerical Thermo-Mechanical Model for the Welding and Subsequent Loading of a Fabricated Structure," *Computers and Structures,* Vol. 3, No. 5, September 1973, pp. 1145-1174.

3. Muraki, T., Bryan, J. J., and Masubuchi, K., "Analysis of Thermal Stress and Metal Movement During Welding," ASME Paper Nos. 74-WA/Mat-4 and 5, presented at the ASME Winter Annual Meeting, New York, N.Y., November 1974.

4. Paley, Z., and Hibbert, P. D., "Computation of Temperatures in Actual Weld Designs," *Welding Journal,* 54 (11), Nov. 1975, Research Suppl., 385-s to 400-s.

5. Glickstein, S. S., Friedman, E., and Yeniscavish, W., "Investigation of Alloy 600 Welding Parameters," *Welding Journal,* 54 (4), April 1975, Research Suppl., 113-s to 122-s.

6. Friedman, E., "Thermomechanical Analysis of the Welding Process Using the Finite Element Method," *Trans. ASME, J. Pressure Vessel Techn.,* Vol. 97, Series J, No. 3, August 1975, pp. 206-213.

7. Wilson, E. L., and Nickell, R. E., "Application of the Finite Element Method to Heat Conduction Analysis," *Nuclear Engr. and Design,* Vol. 4, 1966, pp. 276-286.

8. Zienciewicz, O. C., and Parekh, C. J., "Transient Field Problems: Two-Dimensional and Three-Dimensional Analysis by Isoparametric Finite Elements," *Intl. J. Num. Methods Engr.,* Vol. 2, 1970, pp. 61-71.

9. Friedman, E., "A Direct Iteration Method for the Incorporation of Phase Change in Finite Element Heat Conduction Programs," WAPD-TM-1133, Bettis Atomic Power Laboratory, Pgh., PA, March 1974.

10. Chihoski, R. A., "The Rationing of Power Between the Gas Tungsten Arc and Electrode," *Welding Journal,* 49 (2), Feb. 1970, Research Suppl., 69-s to 82-s.

11. Kopersak, N. I., Slivinskii, A. M., and Dukhno, V. M., "Temperature Conditions in Weld Pools," *Automatic Welding,* No. 7, 1973, pp. 1-3.

12. "Engineering Properties of Inconel Alloy 600," Technical Bulletin T-7, International Nickel Co., Huntington, W. Va., 1964.

13. Schoeck, P. A., "An Investigation of the Anode Energy Balance of High Intensity Arcs in Argon," *Modern Developments in Heat Transfer,* Academic Press, New York, 1963, pp. 353-400.

14. Shaw, C. B., Jr., "Diagnostic Studies of the GTAW Arc; Part 2 — Mathematical Model," *Welding Journal,* 54 (3), March 1975, Research Suppl., 81-s to 86-s.

15. Glickstein, S. S., "Temperature Measurements in a Free Burning Arc," WAPD-TM-1216, Bettis Atomic Power Laboratory, Pgh., PA, September 1975.

16. Carslaw, H. S. and Jaeger, J. C., *Conduction of Heat in Solids.* Oxford University Press, London, 1947, pp. 220-221.

Appendix — Point Source Temperature Solutions

Point Source at the Surface of a Semi-Infinite Space

Consider a continuous point source of heat of strength Q, applied at the origin R = O, of an infinite space defined by R ≥ O in a spherical coordinate system. The spherically symmetric temperature T, at any distance R, from the point of application of the heat source and at a time t, which denotes the duration of heating, is given by Carslaw and Jaeger (Ref. 16):

$$T(R,t) = (Q/4\pi\, k\, R)\ \mathrm{erfc}\ (R/\sqrt{4\,D\,t}) + T_o \qquad \text{(A1)}$$

where k is the thermal conductivity (constant), and D is the thermal diffusivity (constant); erfc is the complementary error function defined by $\mathrm{erfc}(z) = (2/\sqrt{\pi})\int_z^\infty e^{-x^2}\,dx$. It is easily shown that this solution satisfies the transient heat conduction equation

$$D\nabla^2 T = (D/R^2)\,(\delta/\delta R)\,(R^2\delta T/\delta R) = \delta T/\delta t \qquad \text{(A2)}$$

for R > O, and the conditions $T(R,O) = T_o$ and $\lim_{R\to\infty} T(R,t) = T_o$.

For a semi-infinite body defined by z ≥ O in an (r,z) cylindrical coordinate system, such that the plane surface z = O is adiabatic, a continuous point source of heat applied at (r,z) = (O,O) yields exactly the same temperature solution as that given by eq. (A1) for an infinite body, except that all of the heat generated at the source is now conducted into the half-space, rather than the infinite space.

Thus, in cylindrical coordinates,

$$T(r,z,t) = (Q/2\,\pi\,k)\ \mathrm{erfc}\ \sqrt{r^2+z^2}\ \cdot\ \sqrt{1/4\,Dt}\ /\ \sqrt{r^2+z^2} \qquad \text{(A3)}$$

Point Source at the Surface of an Infinite Plate of Finite Thickness

Consider a continuous point source of heat of strength Q, applied at a point with coordinates (r,z) = (O,O) on the surface z = O of a plate of infinite extent and finite thickness h. The surfaces defined by z = O and z = h are adiabatic. The point source solution in a semi-infinite space (eq (A3)), results in non-zero heat flow at z = h. An image source applied at (r,z) = (0,2h) ensures that z = h is adiabatic, but now there is non-zero heat flow at z = O. Another image source applied at (r,z) = (O,-2h) is now required to satisfy conditions at z = O. Carrying this along ad infinitum, an infinite distribution of images of the source is applied at points (r,z) = (0, ± 2 n h), n = 1,2, . . . The solution for a single point source of heat applied at (r,z) = (O,z′) is given by:

$$T(r,z-z',t) = (Q/2\,\pi\,k)\ \mathrm{erfc}\ \sqrt{r^2+(z-z')^2}\ \cdot\ \sqrt{1/4\,Dt}\ /\ \sqrt{r^2+(z-z')^2} \qquad \text{(A4)}$$

The superposition of the semi-infinite solution and the image solution then yields the temperature solution satisfying the adiabatic boundary conditions:

$$T(r,z,t) = (Q/2\,\pi\,k)\sum_{n=-\infty}^{\infty}\mathrm{erfc}\ \sqrt{r^2+(z+2\,n\,h)^2}\ \cdot\ \sqrt{1/4\,Dt}\ /\ \sqrt{r^2+(z+2\,n\,h)^2} \qquad \text{(A5)}$$